Sympathy for the Devil

Investigating the spread and impact of Devil Facial Tumour Disease

Devil CBM Phys Lab

Michael Croft, Adam Owiar, Diego Prieto, Jonah Wilbur

April 4, 2024

ISCI 1A24

Table of Contents

Abstract 3

General Introduction and Background 4

Motivations and Study Approach 13

Study 1 14

- Methods 14
- Results 18

Study 2 22

- Motivations 22
- Methods 23
  - Imaging and Spectroscopy 25
  - Puncture Test 29

Conclusions and Perspectives 30

References 32

- Appendix A 38
- Appendix B 38
- Appendix C 39
- Appendix D 40
- Appendix E 42
- Appendix F 43
- Appendix G 45

Abstract

Cancer has long existed in many organisms beyond humans. Despite its near ubiquitous nature, there exists no singular cure. Devil Facial Tumour Disease (DFTD) in Tasmanian Devils is a unique cancer that can be transmitted through biting of the external tumours and has a mortality rate near 100%. The rapid transmissibility of DFTD, and near certain fatality, places the Devil population at high risk of extinction as their populations have decreased by 83% over the last 30 years[1]. Without human intervention, the wild Tasmanian Devil population may be lost, disrupting Tasmania's delicate food chain and heavily disturbing local biodiversity. Our research goals are to determine how the population dynamics of Sarcophilus Harrisii will change with DFTD as an endemic pathogen and whether there is a chemotherapeutic treatment that can impact transmission and dynamics of DFTD, such that both extinction and a population bottleneck event can be avoided. Our methods are divided into two studies. Study 1 is centered around utilizing compartment-based epidemiological models to project Tasmanian Devil and disease dynamics. Using data from primary and secondary sources, our model has been calibrated to understand DFTD's presence and transmission in a population under any level of chemotherapeutic treatment. This simulation predicted that the population would not go extinct, but the population would be significantly reduced, which could create a population bottleneck event. Analysis of this simulation and its results showed that the level of chemotherapeutic treatment, and its impact on the rate of transmission and tumour progression, heavily determine the proliferation of the disease. This influenced study 2 as we need to investigate our chemotherapeutic drug, Sunitinib malate, for any unforeseen changes to rate of transmission, or side effects that adversely impact the population. A common side effect of sunitinib malate is decreased vasculature; this may have potential to weaken the skin around the tumour, increasing infectivity through decreased tumour integrity when bitten. Our second study necessitates capturing several wild Tasmanian Devils to run tests on. By using Geographical Information System (GIS) data on Devil population sightings we can deduce where to find these organisms in their large habitat range. Assessing tumour vasculature with MRI and using a hydraulic press we can determine skin integrity by comparing bite force required to puncture untreated tumour samples, treated tumour samples, and non-infected skin samples. This information will further inform our model and determine whether sunitinib malate is a viable method of ensuring future genetic diversity in the Devil

population. This study would contribute to promoting biodiversity in Tasmanian Devil populations by reevaluating the efficacy of our treatment and updating our current model to predict a further course of action concerning the conservation of the species.

General Introduction and Background

Sarcophilus Harrisii, or Tasmanian Devils, are the largest species of carnivorous marsupials[2]. Known for their hair-raising nocturnal shrieks, they have experienced numerous trials and tribulations in their evolutionary history; the most recent of which being DFTD. DFTD is a transmissible cancer which primarily spreads through bites[3]. These bites occur almost exclusively during the mating season, when during fights for a mate, dominant male Devils will bite the face and mouth of submissive male Devils and become infected. DFTD originated in a female Devil Schwann cell[4], DFTD has a mortality rate of nearly 100% within 6-12 months of lesion appearance, though rare cases of remission and immunity in female Devils has been studied in recent times[2,5]. The disease manifests as round and/or spindle shaped cancer cells in the dermis which accumulate within the head, neck, and oral cavity. DFTD is highly metastatic, with 65% of cases metastasizing to the lymph node, thorax and abdomen[2]. This rapid progression eventually blocks the Devil's oral cavity, often leading to starvation. The severity of DFTD has led to a population decrease of approximately 80% since 1996 and was initially predicted to cause extinction within 35 years without treatment or control[6]. Recent epidemiological models, however, have predicted that both the extinction of DFTD and its coexistence within the population are other possible outcomes[7].

Transmissible cancers are a rare phenomenon in defiance of the traditional axioms of cancer. Although traditionally viewed as a genetic corruption of a host’s cells, cancer can be viewed as evolution on the cellular scale, where cells specialized to maximize individual reproduction and proliferation. This speciation typically results in the death of the individuals afflicted and the cancerous cells, but in the case of transmissible cancers, the cells may continue within a new host. Transmissible cancers have thus evolved as pathogens and survive much beyond the

lifespans of their original hosts[8]. As a karyotypical cancer, DFTD is speculated to have originated in chromosome 1, when telomeres on one homologue of chromosomes 1 and X became pathologically short, allowing for the fusion of the two chromosomes[9]. This is believed to have caused a cascade of further passenger and driver mutations in proto-oncogenes and regular genes alike, culminating in the transmissible, malignant properties of the cancer. Since its discovery in the mid 1990s, two separate DTFDs have been identified, each with their own unique genetic markers that are not related to the host[9]. Though the exact mechanisms driving tumourigenesis have not been pinpointed, from observations of the telomeric mutations it may be drawn that a loss of function mutation is the original oncogenic mutation driving the cancer. This is further corroborated by the downregulation of the Major Histocompatibility Complex (MHC) in cancerous cells. The MHC is a complex of proteins located on the outer membrane of cells and allows immune cells to detect abnormalities in protein production within the cell[10]. MHC genetic diversity among Devils has been observed to be historically low, much before the arrival of DFTD, which most likely contributed to the susceptibility of Tasmanian Devils to the first cases of DFTD[6]. Polymorphism in the MHC has been shown instrumental to foreign tissue rejection, and thus the low MHC diversity in Devil populations facilitates the acceptance of foreign cancer cells in DFTD[2,10]. MHC peptide complex 1 (MHC1) is specifically affected in DFTD cells. MHC1 is located within cells and is responsible for detecting abnormalities inside the cell and bringing them to the surface so they may be detected by the immune system. Without the expression of MHC1, healthy immune systems cannot destroy the cancer, as they have nothing to detect. MHC1 is present in DFTD cells; but severely downregulated[7]. This is likely due to the upregulation of the ERBB-STAT3 axis (erythroblastic leukemia viral oncogene homologue - signal transducer and activator of transcription 3 axis), which is prevalent in DFTD. ERBB-STAT3 is a protein complex upstream of histone deacetylase; which epigenetically silences genes associated with MHC1 regulation such as β2m, TAP1, and TAP2[11] which prevents MHC1 expression in the cancer. Thus, to restore MHC1 expression, the ERBB-STAT3 axis must be disrupted, either by downregulating STAT3 or ERBB. Here, we present a treatment that targets STAT3, to investigate whether there is a chemotherapeutic drug available that can slow the mortality rate of Devil Facial Tumour Disease to promote genetic diversity in Tasmanian Devil populations.

Chemotherapeutic Background

Sunitinib is a multi-kinase inhibitor which targets several receptor tyrosine kinases (RTKs)[12]. In our proposed treatment, we would use SUTENT®, an orally administrated malate salt of Sunitinib. Once swallowed, the drug will travel to the stomach where it reacts with hydrochloric acid. Since this interaction involves a strong acid reacting with an organic compound, the acid will react with the weakest bond that exhibits basic character (Equation 1). In this compound, the presence of aromatic structures heavily determines the overall stability of the compound. The three criteria for aromaticity include the structure being cyclic, the atoms being sp^2 or sp hybridized, and π bonded electrons following Hückel's rule. Groups A and B (Equation 1) are connected by sp or sp^2 bonds, are cyclic, and contain a total number of π bonded electrons equal to 4n+2. This is in accordance with Hückel's rule, making them aromatic structures. These groups are very stable and allow sunitinib to maintain its structure within the body[13].

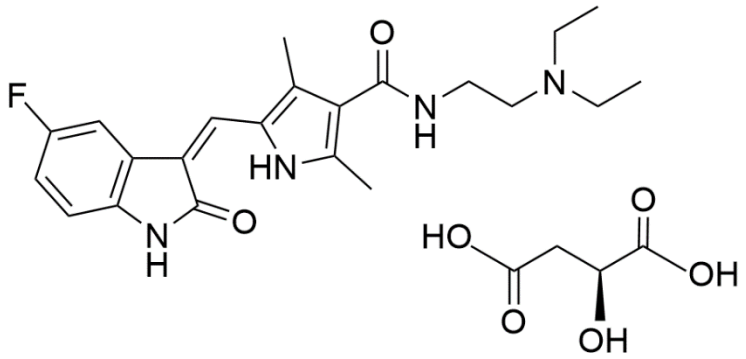

Sunitinib Malate

Figure 1. The chemical structure of the pharmaceutical salt sunitinib malate. The compound to the left is sunitinib and the compound to the right is malate. The full chemical name of sunitinib malate is Butanedioic acid, hydroxy-, (2S)-, compound with N-[2-(diethylamino)ethyl]-5-[(Z)-(5-fluoro-1,2-dihydro-2-oxo3H-indol-3-ylidine)methyl]-2,4-dimethyl-1H-pyrrole-3-carboxamide[11] . F*igure created on ChemDraw by Owiar.*

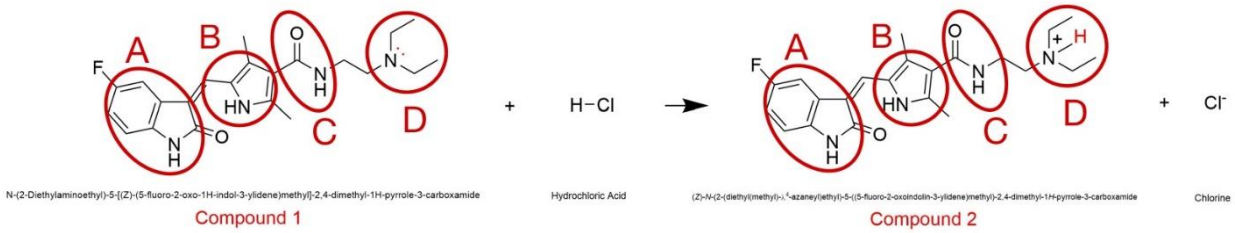

Figure 2. Sunitinib malate is the complete compound provided to the patient; however, the active ingredient is sunitinib as shown in the reaction below the compound. The reaction shown is between sunitinib and hydrochloric acid. The organic compound nomenclature for compound 1 and 2 is below each respective structure. The structure of this compound is essential to its stability and reactivity. Key components are circled as group A, B, C, and D. As noted, the lone pair from compound 1 group D breaks the hydrogen bond in hydrochloric acid. The hydrogen post reaction is bonded to the nitrogen in group D, compound 2, ultimately creating a mildly acidic positive nitrogen compound[14]*. Figure and compounds made in ChemDraw by Owiar.*

The amide present in the structure is known to be neutral[15], however, group D is a nitrogen with a single lone pair. The presence of a lone pair on nitrogen defines the nitrogen as a Lewis base, as well as a nucleophile since it can accept a proton- ultimately making this component basic. Group D acts as a nucleophile and undergoes nucleophilic substitution with the hydrochloric acid. The overall stability of Sunitinib allows the compound to undergo decreases in environmental pH without the fundamental properties of the compound changing. The log of sunitinib's octanol/water distribution coefficient value is 5.2, which is the ratio between octanol/water. Since the value is greater than one, the compound is more likely to dissolve in fats relative to water. This allows the drug to pass through phospholipid bilayer and easily penetrate lipophilic layers and enter the bloodstream. Once past the stomach, sunitinib is metabolised by the enzyme CYP3A4, which breaks it down into its primary/active metabolite SU012662 which is further metabolised into inactive compounds[16] (Figure 3). Both sunitinib and its primary metabolite are therapeutically active.

The optimal dosage is determined by analyzing how quickly the compound can be absorbed, at what quantities it is beneficial, and how it is eliminated from the body. The loading dose for a treatment is meant to get patients within the therapeutic range, which is the concentration range in which the drug is most effective in the shortest amount of time. By multiplying the volume of distribution and the steady state concentration required, the loading dose is calculated to be 237 mg for the average human, as shown in Figure 3 (*Appendix A*). This is also the upper limit of the therapeutic range with 148mg (*Appendix B*) being the lower limit.

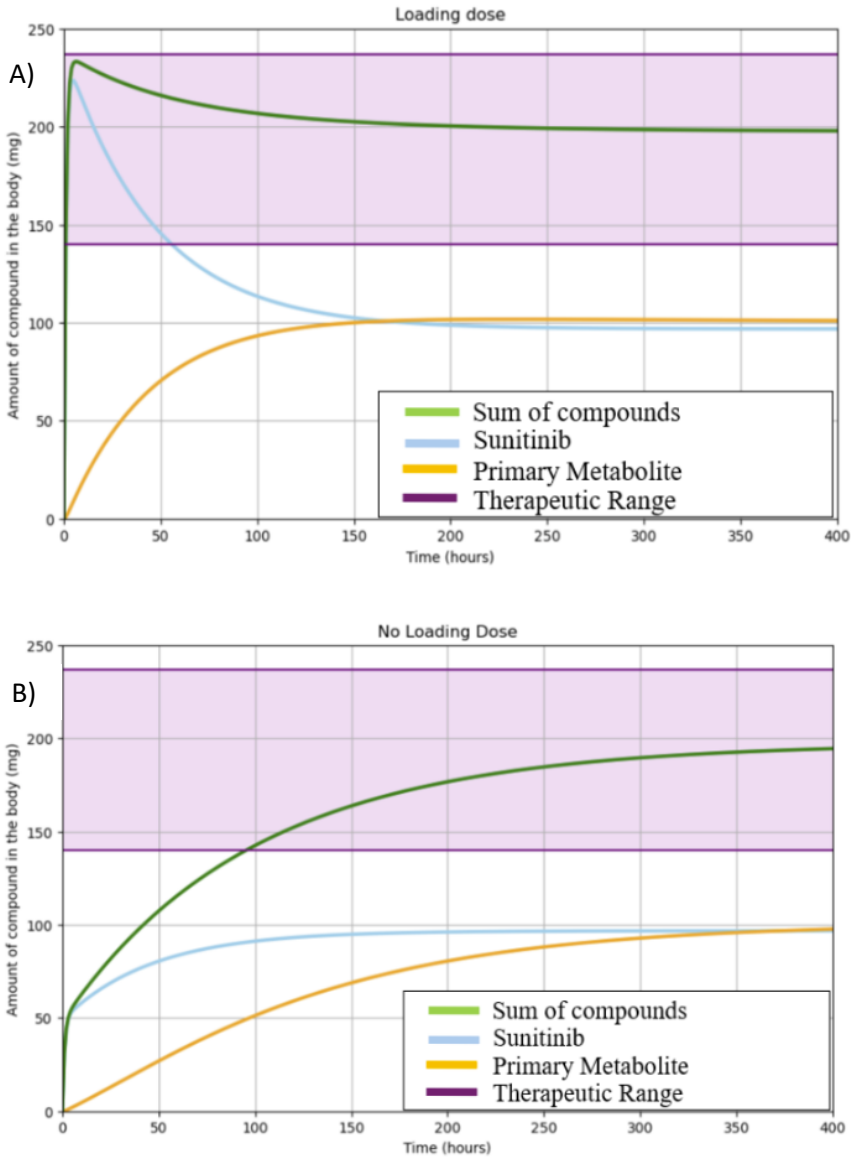

Figure 3. Pharmacokinetic model of sunitinib doses acting in the body. Graph A incorporates the loading dose with the required maintenance doses, while graph B is the regularly prescribed doses. The -Axis is milligrams of compound in the body while the x-axis is time in hours. This simplified model made in python is a compartment-based model which incorporates various drug interactions with the body, those interactions being absorption, distribution, metabolism, and excretion (ADME)[17(p1)]*. Figure created by Wilbur and Owiar (Appendix D).*

95% of Sunitinib is first absorbed through the intestinal mucus membrane and taken into the body's circulation. Distribution describes how the drug is spread through a medium. A

pharmaceutical's volume of distribution is the ratio between the amount of the compound in the body, and its concentration in the plasma. Each compound has its own volume of distribution, sunitinib's being 2230 L and its primary metabolite's volume being 3080 L[18]. Excretion is modelled by average clearance rates with sunitinib's being 48 L/hr and its metabolite's being 29.6 L/hr. ADME interactions are broken up into compartments where the hourly dose is absorbed into the body then moved into the gastral intestine. From there, sunitinib partly forms a metabolite and both compounds get further absorbed, distributed, and cleared from the system. The combination of ADME in sunitinib and its metabolite is what brings the drug into the therapeutic range highlighted in purple on the graph.[11] As shown in graph A, the loading dose enters the therapeutic range within the first hour and remains there for the entire simulation. Comparatively graph B enters the therapeutic range after approximately 110 hours. The time is projected over the course of 400 hours, as 336 hours is the maximum time it takes to reach steady state concentration with the therapeutic range being the same as min and max loading doses. Steady state concentration can be noted when the combined function of sunitinib and its primary metabolite have an approximate slope of zero.

Taking this dose and the required maintenance doses of 6.63mg/h (*Appendix C*), a steady state concentration within the therapeutic range is achieved in 10-14 days[11]. The normal prescribed dose for humans is 50mg per day over the course of 28 days, with the steady state concentration also being reached in 10-14 days[16] . The loading dose compared to the average prescribed dose brings sunitinib to a higher steady state concentration, but also reaches the therapeutic range approximately 110 hours faster than the regular prescribed dose (Figure 3). This means the loading dose can allow effective treatment right away and have a 110-hour head start than the prescribed dose leading to a faster recovery[19].

A lower repeated dose may lead to a longer recovery, however, it is significantly safer to limit symptoms inflicted on the individual which has extended implications for treating Tasmanian Devils. Sunitinib ingestion is associated with acute side effects including diarrhea and nausea, but by taking smaller doses of 50mg at a time, this provides more time for human homeostatic equilibria to adapt to the high concentrations. In our treatment, we propose scaling down the 50mg doses for humans, to 3.76 mg of Sunitinib malate to accommodate for the Tasmanian

Devil's lower body mass, in combination with 0.0235 mg Imodium to treat diarrhetic and emetic symptoms (dose adjusted from human trials by average body mass) for four weeks during the mating season where transmission rate is at its peak.

Sunitinib is an antagonistic drug, since it binds to the receptors that upregulate STAT3, which as previously mentioned downregulates MHC1. By downregulating the down-regulator of MHC1, Sunitinib indirectly increases its expression. This downregulation serves to eliminate; not reverse or increase the receptor kinase activity. The specific receptor kinases responsible for MHC1 downregulation, as well as angiogenesis, that sunitinib targets are the Vascular Endothelial Growth Factor Receptor (VEGFR) and Platelet-derived Growth Factor Receptor (PDGF)[20]. In the absence of angiogenesis, tumour cells will experience hypoxia and will be limited in size[21]. VEGFR is a receptor tyrosine kinase responsible for neovascularization in tumour cells, being almost ubiquitously expressed in cancers. VEGF activates signaling in endothelial cells (EC) after binding to cognate receptors on the cell surface, driving angiogenesis[22]. VEGFR 1 and 2 are its tyrosine receptors, which sunitinib inhibits by binding to the VEGFR2 receptor, inhibiting its phosphorylation[21]. Competitively inhibiting the tyrosine receptors of VEGF leads to the consequential inhibition of VEGF activation itself through a multitude of downstream inhibitors in the EC, such as Steroid Receptor Coactivator (SRC). VEGFR2 is responsible for the characteristic effects of VEGF on the EC, such as cell proliferation, chemotaxis, and vascular permeability. According to Chen et al's study on the relationship between VEGF and STAT3, it was found that STAT3 is activated by phosphorylation upon VEGF stimulation in EC in vitro and in vivo by a VEGFR2 and SRC dependent mechanism. Furthermore, STAT3 mediates Bcl-2 (a gene that regulates cell death) activation by VEGF[22]. Thus, STAT3 may be downregulated indirectly by targeting VEGF through its second receptor kinase, which sunitinib inhibits. Angiogenesis may also be reduced by sunitinib through the direct inhibition of VEGF.

The PDGF family includes the most comprehensive phenotype-moderating agents, among which PDGF-BB is the most relevant to disease as it is the only member of the PDGF family that may bind to the dimers of both PDGF proteins, PDGFRα and PDGFRβ[23]. Sunitinib inhibits PDGF by a similar mechanism of action to how it inhibits VEGF; it blocks the PDGFRβ receptor phosphorylation[21]. One downstream effect of the overactivation of PDGFBB is the suppression

of miR-1181[24]. miR-1181 is a MicroRNA; a family of noncoding 17-25 nucleotide-long RNAs that regulate the expression of multiple genes post-transcriptionally. It has been found in recent studies that miRNAs can function as tumour suppressors[25]. It was discovered by Wang et al's study that the overactivation of miR-1181 inhibited the expression of STAT3, while it's downregulation up-regulated STAT3, though the exact mechanisms of this function are unknown[24]. Thus, it can be determined that the inhibition of PDGF through sunitinib may downregulate PDGFBB, upregulating miR-1181 and finally downregulating STAT3, which upregulates MHC1, that being the goal of treatment. The overall mechanism of action of sunitinib is shown in Figure 4.

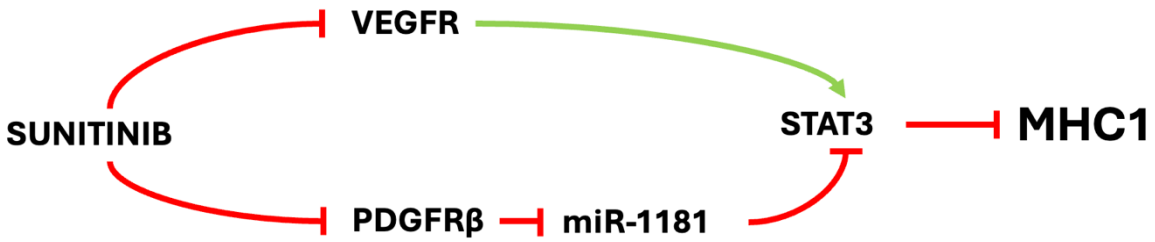

Figure 4. Flow chart demonstrating the mechanism of action of sunitinib. Red arrows represent downregulation, while green arrows show upregulation. Since the VEGFR pathway shows one upregulation arrow and two downregulation arrows to MHC1, sunitinib indirectly upregulates MHC1 through VEGFR. Since the PDGFRβ pathway shows four downregulation arrows to MHC1, sunitinib also indirectly upregulates MHC1 through PDGFRβ. Figure created by Croft.

All in all, the downregulation of STAT3 through these routes using sunitinib malate SUTENT® provides a treatment of DFTD. SUTENT®, however, is not a silver bullet. Pitfalls, such as the need to dose daily and temperature requirements may be accounted for in the design of our treatment model and strategy, though the adverse side effects of the drug need to be considered in more detail. STAT3 is a transcription factor that has a proliferative effect on many different cell types[26]. Since gut cells must frequently proliferate, STAT3 inhibition may adversely affect gut health, causing many side effects to the sunitinib medicine. Gastrointestinal issues such as weight loss, dyspepsia, flatulence, bloating, nausea and vomiting were listed as

sunitinib therapy side effects by Schwandt et al's study[27]. These side effects may adversely and exponentially confound with the negative metabolic effects associated with the cancer, and so these externalities must be treated or the sunitinib therapy may not be an effective treatment. Thus, 0.0235 mg Imodium, an antidiuretic, will be used to treat the gastrointestinal side effects of sunitinib. All in all, the combined administration of SUTENT® and Imodium will be utilized to treat DFTD.

Motivations and Study Approach

The Tasmanian Devil species has undergone multiple bottlenecks within their evolutionary history, including DFTD. As with many insular species, Tasmanian Devils have a distinct lack of genetic diversity, manifesting in low diversity in the microsatellite, mitochondrial-nuclear and immune system genes[1]. It is thought that the culprit of the Devil's low genetic diversity lies in the following four factors: environmental change in the last glacial maximum, El Nino Southern Oscillation (ENSO), Europeans settlement of Tasmania, and finally, DFTD. The first bottleneck, the glacial maximum, occurred about 20,000 years ago, where cool temperatures replaced conventional vegetation with grassland and open scrub, which decreased prey distribution and therefore the Devil population. The second bottleneck, the ENSO, lead to a drier climate with frequent droughts, which also decreased prey abundance and therefore the Devil population. The third bottleneck was the extensive bounty hunting of the Devils by European settlers. The fourth struggle is the DFTD we are studying. The Devils have also experienced a recent founder effect as they migrated from Australia to Tasmania[28]. In understanding the mechanisms behind these depletions of genetic diversity we can observe how the Devils have overcome and survived evolutionary pressure, as well as why we might be inclined to help them succeed their current epidemic. What the species past challenges have in common is that they were overcome by the Devils. DFTD, however, is still ongoing. The species' genetic diversity had already been so depleted by the aforementioned events that they were especially prone to developing the cancer[2]. The Devil's current dilemma is thus a case study not only in the unique and challenging transmissible cancer, but in the importance of genetic and biodiversity. This is why it is more than worthwhile studying the mechanisms effects of the cancer system as well as how we might treat it. In two studies, we investigate the disease-treatment population dynamics (Study 1) and

explore the effects of our treatment on physiological characteristics of individual Devils (Study 2).

Study 1

Methods

Compartment based models are used to describe and investigate infectious disease, to inform both preventative and remedial strategies of disease management[29]. A common question that compartment-based models seek to address is if there's potential for an outbreak, and the effects of said outbreak. Our study seeks to identify what the results of the initial outbreak will be, and what would happen in the case of re-introduction of the pathogen to a disease free population. Compartment based models can become increasingly complex by incorporating more compartments to represent various disease-related states. These models function by separating the population into compartments distinguished by relevant characteristics, where individuals move between compartments at varying rates. Compartments might include separate infected, exposed, and deceased populations. In designing a compartment-based model, predictions and assumptions must be made with regards to the disease and treatment's dynamic effects on the overall population; this is done to choose to the specific compartments as well as their interactions and flows. This model can then be investigated numerically and provide quantitative data on how the population in each compartment is predicted to change over time. Compartment based models are effective at investigating the size of the total population and in monitoring gross population changes over long periods time using minimal computing power[29].

Our model is based on the susceptible-infectious-exposed-recovered (SEIR) model. Our model seeks to investigate the population dynamics of Tasmanian Devils after the introduction of DFTD in 1996. Although originally thought to threaten Devil extinction[6], recent studies suggest that the disease could reach an equilibrium in the population or could die out completely[7]. Our model uses compartments for the susceptible, exposed (but not yet infectious), infectious and recovered sub-populations of the Devils (Figure 5). The transmission rate, ε, is highly time dependent as transmission occurs primarily through biting in male sexual competition during the mating

season in March. This rate is controlled by the base parameter ε, and a scaling function f_s to scale the rate of transmission, increasing it during mating season.

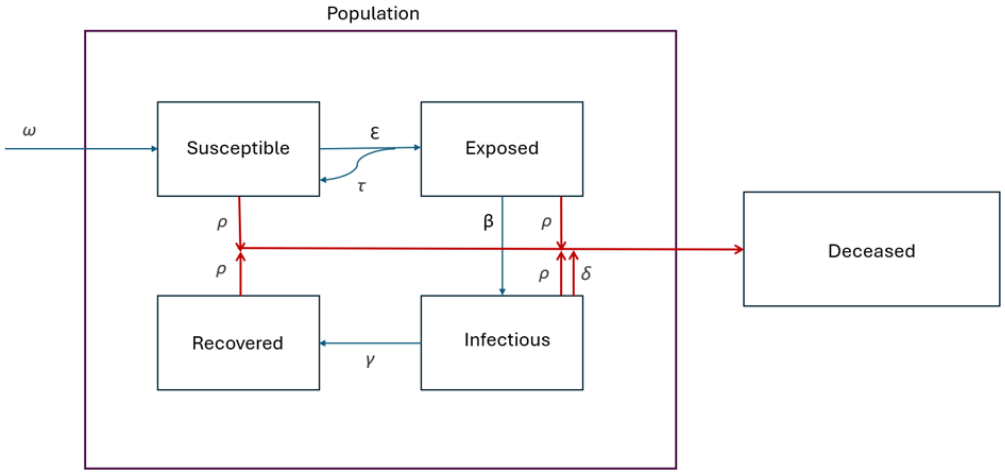

Figure 5. Box model of the compartment-based study. Blue arrows indicate flows between compartments and red arrows represent flows that are leaving the population (death). Boxes represent the individual compartments in the model Figure created by Wilbur.

$$\frac{dS}{dt} = \omega N - \frac{\epsilon f_s I S(1-\tau)}{N} - \frac{\rho S N}{K} \quad (1)$$

$$\frac{dE}{dt} = \frac{\epsilon f_s I S(1-\tau)}{N} - (1-0.5\tau)\beta E - \frac{\rho E N}{K} \quad (2)$$

$$\frac{dI}{dt} = (1-0.5\tau)\beta E - \delta I - \frac{\gamma I - \rho I N}{K} \quad (3)$$

$$\frac{dR}{dt} = \gamma I - \frac{\rho R N}{K} \quad (4)$$

Equations 1:4. The equations defining the rates of change in each compartment of the model, S, E, I and R.

Though our model stems from the commonly used SEIR model, we have an additional counter for the total population (P) and total deceased (D). The former is a sum of each susceptible, exposed, infected, and recovered individuals. The latter is the total number of Devils deceased both naturally and due to DFTD. Natural birth and death rates must be considered since the disease spans multiple generations, and so the cancer dynamics will be affected by these rates. Our model is based off known ecological data, such as population size, natural death rate and disease mortality rate[5,30]. These factors and their interactions were then carefully considered to make an accurate model.

To begin, the susceptible compartment represents the subset of the population that have not yet contracted DTFD, making them non-infectious and prone to contracting the cancer. The number of individuals in the susceptible compartment will be increased by the birth rate, ω, and the treatment's rate of remission, τ, which brings the Devils from the exposed compartment back to the susceptible compartment. The compartment is reduced by the natural death rate, ρ, which brings the Devils to the deceased compartment, and the rate of exposure, ε, which brings the Devils to the exposed compartment.

The exposed compartment represents the Devils who have contracted DFTD, but whose tumours have not yet grown large enough to be infectious, since infectivity is related to tumour size[3]. This property emerges from the mechanism of transmission; Devils that bite the mouths and faces of infected Devils are infected with the cancer as it acts as an allograft from the old host. This compartment is increased by ε and decreased by ρ and the cancer progression rate β, which represents the flow of Devils from the exposed to infectious compartment.

The infected compartment represents Devils whose cancer has progressed to the point where they are considered infectious to Devils biting their mouths or faces. This compartment is increased by β, and has outputs of ρ, the disease mortality rate δ, and the recovery rate γ. It is worthwhile to note that the recovered subset includes a small subset of Devils who recovered without treatment, though this number is exceedingly small relative to the population[5].

The recovered compartment represents the Devils that have contracted the pathogen but become immune. It is added to by γ, which moves the Devils from infectious to recovered, and reduced by ρ, which moves the Devils to the deceased compartment. This compartment-based model

allows us to answer our specific research questions by evaluating both the population changes over long periods of time and evaluating the effect of treatment τ on the population. This model seeks to determine whether the population will go extinct without any intervention, and what the minimum amount of treatment would be for the cancer to be eliminated from the population.

The parameters ω, ρ, δ, γ, K, and f_s were calculated using known ecological data[5,30], and the parameter τ is target portion of the population being treated. f_s is a time dependent scaling parameter, meant to adjust the transmission factor ε to the behaviour of the Devils[31]. f_s was fit to the data depicting mating behaviour of Tasmanian Devils using a truncated Fourier series[31]. ω was calculated from the natural birth rate of Tasmanian Devils in the wild[30]. ρ was determined to be the same value as ω, but multiplied by the population divided by K (the carrying capacity), to account for logistical population growth. δ was calculated as the probability that any Devil with a tumour dies each day, given that ~100% die within 6-12 months of developing a tumour[7]. γ was determined to be a very small, positive, non-zero number since some Devils are in remission following immune responses to the tumour. This number of Devils is extremely small in comparison to the total population that has contracted DFTD in the known lifetime of the pathogen[5]. The carrying capacity was assumed to be the equilibrium population of the Devils prior to introduction (53000)[32].

Due to lack of available data on the rate of tumour progression in Tasmanian Devils, β and ε were adjusted to fit the model to known population data given the other parameters[7].

The fixed parameters were determined to be $\omega = 0.0016$, $\rho = 0.0016$, $\delta = 0.0021$, $\gamma = 0.00001$, $K = 53\,000$, $\beta = 0.02$, $\varepsilon = 0.015$. τ is variable, and also equal to the portion of the population that is treated.

Results

Our model predicts that given the current population of Devils, and the interpolated parameters of the disease dynamics, the population will reach a pseudo-equilibrium with DFTD in the absence of treatment in about 30 years (Figure 6).

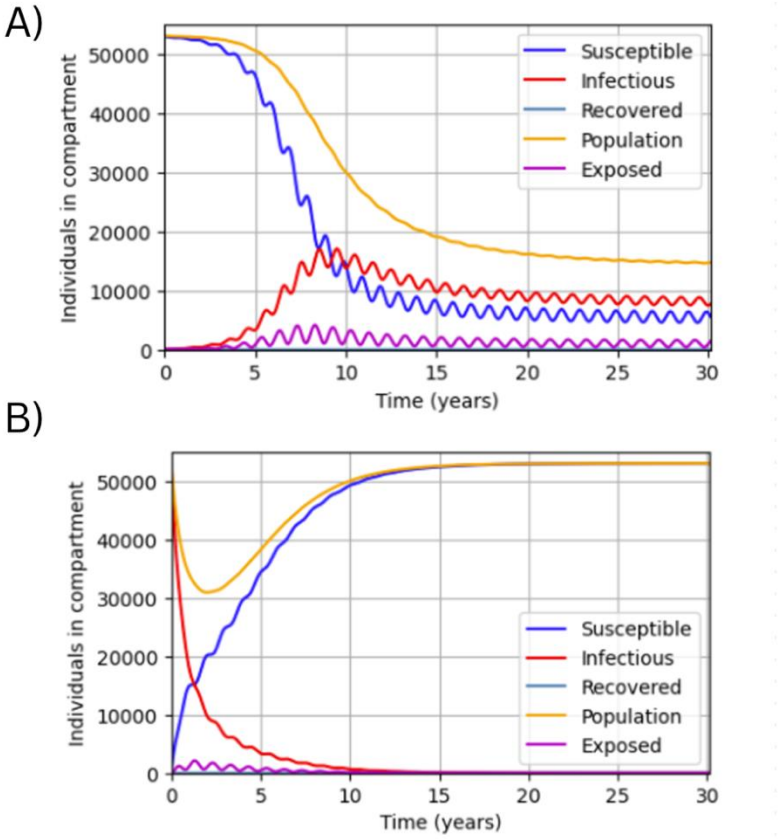

Figure 6. Graphs displaying the population in different compartments in the model over time, with A) τ = 0, initial infections = 100, and B) τ = 0.67, initial infections = 53 000, whose significance is explained below. The x-axis is the time in years since the start of the simulation, the y-axis is the number of individuals in each compartment. In both, the yellow line represents the entire population, the blue line represents the population that is susceptible to the disease, the red line represents the population that is infectious, and the purple line represents the population that has been exposed but is not infectious. The sinuosity observed in these graphs are due to the periodic mating behaviours of Tasmanian Devils that impact both disease transmission and life-cycle changes. Figure created by Wilbur. (Appendix E)

Though this indicates that Tasmanian Devils will not become extinct, it does leave the population prone to bottleneck effect-events and would also result in an even less genetically diverse population. DFTD was originally able to ravage the population due to a population bottleneck event in the Mid-Holocene, resulting from limited food, climactic fluctuations and European settlers disrupting the ecosystem[33]. Additionally, DFTD has created another large bottleneck, where the population is 15% of what it once was, which promotes inbreeding, decreases heterozygosity, and leads to population drift where small random fluctuations could have long-lasting and potentially deleterious effects on the future population[34]. Since we predict that the population will not become extinct, it is more imperative to genetic diversity, since the lack of genetic diversity is what allowed for DFTD in the first place. As such, it would be worthwhile to continue to explore a treatment plan for the Devils that would eradicate this disease nonetheless, because a smaller population will have inherently reduced genetic diversity[34].

The basic reproductive number ($\mathcal{R}_0$) of an infectious disease is useful to help determine effective methods of treatment and management. It is defined as the number of individuals that any given individual will infect after being infected[35]. An $\mathcal{R}_0$ value greater than 1 indicates that the disease will spread and survive within a population, whereas an $\mathcal{R}_0$ value less than 1 indicates that the disease will go extinct, over one or more generations. The $\mathcal{R}_0$ function of our model was calculated using the next generation matrix method (NGM)[35] (Appendix F). The NGM method involves creating a matrix (Fi) of the new infections in each compartment, and another matrix (Vi) comprising the other flows between compartments. Two new matrices are defined as F and V, those being Jacobian matrices of Fc and Vc respectively. The basic reproductive number ($\mathcal{R}_0$) of an infectious disease is useful to help determine effective methods of treatment and management. It is defined as the number of new infections that will come from each infected individual[35]. An $\mathcal{R}_0$ value greater than 1 indicates that the disease will spread and survive within a population, whereas an $\mathcal{R}_0$ value less than 1 indicates that the disease will go extinct, over one or more generations. The $\mathcal{R}_0$ function of our model was calculated using the next generation matrix method (NGM)[35]. The NGM method involves creating a matrix (Fi) of the new infections in each compartment, and another matrix (Vi) comprising the other flows between compartments. Two new matrices are defined as F and V, those being Jacobian matrices of Fc

and Vc respectively. By substituting the disease-free equilibrium population values into these matrices for the values representing the individuals in each compartment, we can evaluate whether the pathogen could invade a disease-free population. The product of F and the inverse of V is a new matrix labelled K, who's greatest and in our case only, eigenvalue is the expression for $\mathcal{R}_0$[35,36]. By substituting the disease-free equilibrium population values into these matrices for the values representing the individuals in each compartment, we can evaluate whether the pathogen could invade a disease-free population. The product of F and the inverse of V is a new matrix labelled K, who's greatest and in our case only, eigenvalue is the expression for $\mathcal{R}_0$[35,36]. Our calculated $\mathcal{R}_0$ value for this epidemic is determined to be time dependent, as shown in Equation 5 where f_s is a periodic function of t.

$$\mathcal{R}_0 = \frac{\beta \epsilon f_s k^2 (1 - 0.5\tau)(1 - \tau)}{(N\rho + k\delta + k\gamma)(N\rho - 0.5k\beta\tau + k\beta)} \quad (5)$$

Equation 5: Displays the expression found for $\mathcal{R}_0$ in the previously stated model using the next generation matrix method. Parameters are explained in text.

The time dependency is a result of the impact of the mating season on Devil behavior that results in infection. The disease is primarily transferred through bites, and Devils bite each other substantially more when competing for mates during mating season. This behavior suggests that the $\mathcal{R}_0$ will be higher during the mating season and lower outside. The model assumes a periodic increase in behaviors resulting in transmission during the mating season and decrease outside the mating season. The time dependency of $\mathcal{R}_0$ means that the number of other individuals that we can expect any one individual to infect after being infected, depends on the time at which they are infectious. $\mathcal{R}_0$ as a function of time is plotted in Figure 7.

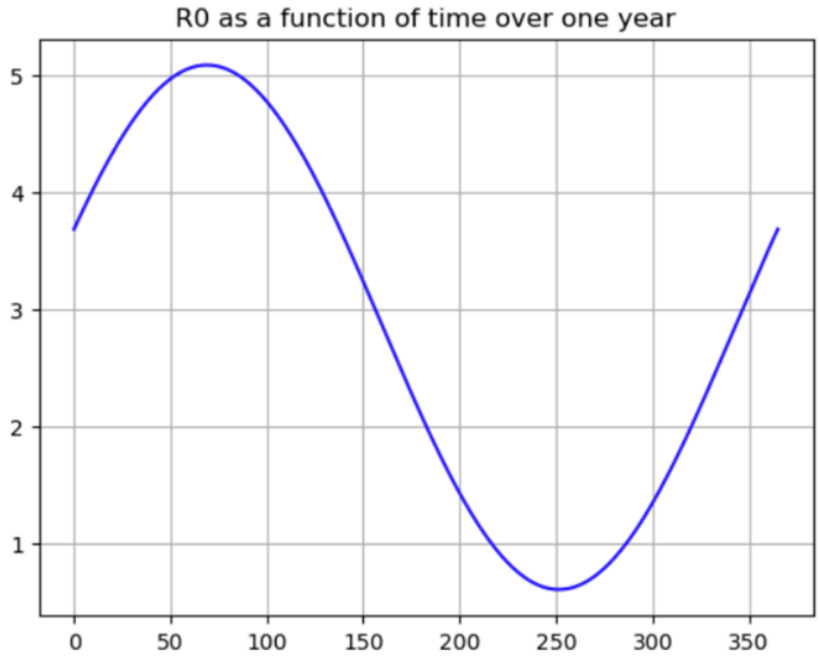

Figure 7. The blue line represents the $\mathcal{R}_0$ value for DFTD, and the x-axis is the number of days since January 1. The y-axis is the value of $\mathcal{R}_0$. Shows that $\mathcal{R}_0$ varies between 5 and slightly less than 1. Figure created by Wilbur.

The $\mathcal{R}_0$ value is also linearly dependent on the population that is treated. As previously mentioned, to ensure a pathogen will become extinct, the $\mathcal{R}_0$ value must be less than one. For this time-dependent function, we found that the average over one year must be less than one, such that over each year there is a net decrease in infection, to ensure elimination of the disease. This model still displays a surge of cases after each mating season before the disease becomes extinct, but shows the disease is eventually eradicated. This minimum level of treatment is 67% (Figure 6 B) of the population, to completely eradicate the disease under any conditions.

When isolating the population at any point in time, with any given treatment, you can determine the $\mathcal{R}_0$ and thus the possibility of resurgence of the disease under those conditions. This allows us to determine the points at which the disease would or would not be able to invade the population upon reintroduction, at a given point of year and treatment. As mentioned earlier, the minimum treatment to avoid re-invasion of such a disease, is 67% if maintained for the whole year but 82% if reintroduction and treatment occur solely during the mating season. This is where the average of $\mathcal{R}_0$ across the time span is less than one. Conversely, if the disease is reintroduced at the lowest

point of transmission, the disease would not spread because with no treatment, the $\mathcal{R}_0$ value is still less than one. The expression for $\mathcal{R}_0$ shows that the influence of the potential treatment is very important to limiting spread of the disease, which will be investigated in study 2. The results of study 2 could then better inform the mathematical model, leading to a potentially more accurate predictive model, allowing us to answer the research question better.

Study 2

Motivations

Study 1 informed us of the drastic periodic changes in transmissibility, expressed in the time dependent function for $\mathcal{R}_0$, of DFTD. Study 1 also informed us of the importance of treatment for promoting genetic diversity between Tasmanian Devils. Although this could have been inferred by the nature of DFTD's transmission, Study 1 quantified this discrepancy and solidified the importance of treatment, which will be practiced in Study 2. Study 1 additionally informed us of the minimum proportions of the Devil population requiring treatment to eventually eradicate DFDT, although these proportions, and our mathematical model, may be subject to change following data from study 2.

Study 2 will examine the effects of our chemotherapeutic and its potency in tumour suppression and impact on tumour ripping, in a controlled environment, monitoring infected and treated Devils in captivity over time. Additionally, we propose using MRI to measure and compare the vascularization of untreated and treated tumours to make predictions on the effects of epithelial integrity in the Devils. Since insufficient vasculature can cause the sloughing of the skin[37], and our tumour treatment targets the upregulation of the MHC-1 complex and downregulation of angiogenesis as it's mechanisms of action, the drug may cause structural damage to the Devil's skin around the tumour. As DFDT is primarily spread through biting, weaker tumour epithelia may lead to easier puncture and thus higher transmissibility. Assessing the efficacy of our chemotherapeutic on tumour suppression and its potential to increase transmissibility through decreased tumour integrity, the overarching viability of our treatment and methods can be determined. Additionally, results from study 2 may contribute to model adjustment, specifically

in the transmissibility parameter, to inform more effective proportions of treatment and thus DFDT eradication.

Methods

To assess the effects of Sunitinib on DFTD, Devils from four separate demographics will be isolated in captivity, and the effects of Sunitinib on vasculature will be detected using two methods. We will use MRI to make qualitative and quantitative measurements of vascular tissue across the four demographics and a tissue shear strength test to quantitively measure tissue strength. We will then evaluate whether there is a correlation between vasculature and tissue strength. We will also evaluate if sunitinib has a significant effect on both vasculature and tissue strength. The first group will be DFTD negative and untreated, to serve as a control. The second group will be DFDT negative and treated, to assess the potential side effects of sunitinib and our methods of treatment on Devils. The third group will be DFTD positive and untreated, to monitor the progression of untreated DFTD. The fourth group will be DFTD positive and treated, to assess the effects of Sunitinib on tumour progression.

In order to confirm which Devils are infected, we will test for the antibody periaxin using methods outlined in Tovar et al's study[38]. In their research on DFTD-tumour specific diagnostic markers, they found that periaxin was the most sensitive test for the cancerous Schwann cells. Periaxin is a marker of myelinating Schwann cells, and in all cases periaxin labelling was moderate to strong in the cancerous cells. This means that by using immunohistochemistry and immunofluorescent strategies outlined in Tovar et al's study, we can determine which Devil cells test positive for periaxin and are thus DFTD cells. As such, we may choose the third and fourth groups of the study to be positive for DFTD using these methods.

To create the second and fourth (treated) groups, we will administer the sunitinib treatment for the proposed duration of treatment (4 weeks to cover the mating season) and ensure the Devils have absorbed the proper levels of the drug. This will be done with a simple urine test, with the expected amounts of Sunitinib being 16% of the given dose[11]. This may be done by utilizing Rodriguez et al's study on the quantitation of Sunitinib and its metabolites in urine[39]. In their study, Sunitinib and it's metabolite N-desethyl Sunitinib were measured in urine by using a nonaqueous-capillary electrophoresis method with TOF-MS. TOF-MS, or time of flight mass

spectrography is a technique used to determine composition of a substance by taking advantage of the principle that ions with the same kinetic but different mass-charge ratios move at different velocities in a magnetic field[40]. Urine was diluted 1:10 to avoid ionic suppression, and separation of compounds was achieved using a 5 mM ammonium formate in methanol. Detection limit was as low as 0.07 mg/L for Sunitinib and 0.15 mg/L for N-desethyl Sunitinib, with experimental accuracy ranging from 96.0 to 100.4%. As this method was designed for routine clinical practice, it is an ideal candidate for our study. With use of Rodriguez et al's methods in Sunitinib detection, as well as Tover et al's studies in DFTD detection, we may differentiate between our four respective study groups.

As Devils are solitary animals with highly dynamic territory ranges of 13-34 km^2, collection of Devils may be difficult or time inefficient[41]. To reduce this, the collection of Devil study subjects can be informed by analyzing Devil sighting density as an analog to population density using a Geographic Information System. QGIS was used to create a heatmap of these sightings to visually represent this density (Figure 8).

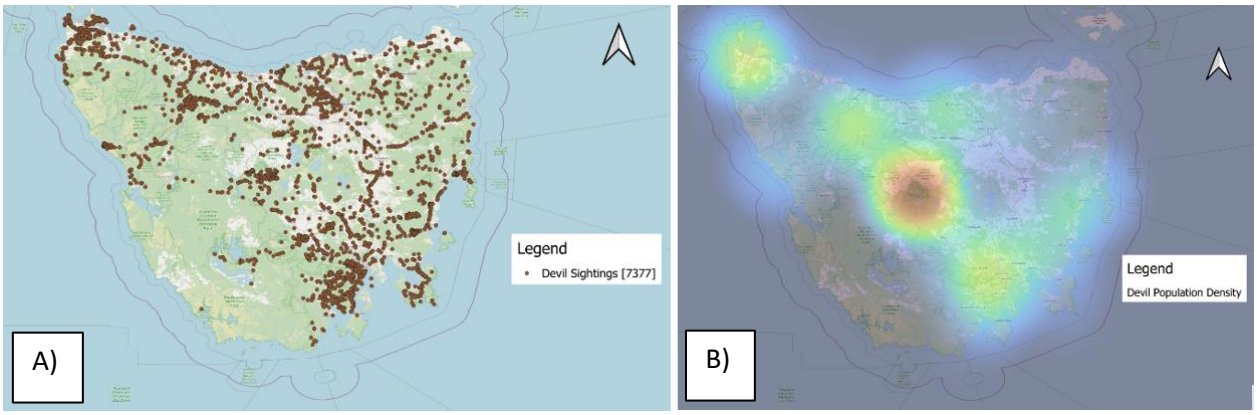

Figure 8: A) A map of verified Tasmanian Devil sightings from January 1, 2018 to January 1, 2023. Each dot represents a single sighting. B) A heatmap of Tasmanian Devil sighting density to aide visualization. Data sourced from the Natural Values Atlas[42]. Figure created by Prieto.

It must be understood that this is a poor representation of actual Devil population distribution, as sighting frequency and location is influenced both by Devil and human position. However, this data is still useful for Devil capture, as regions of high sighting density are more likely to contain

Devils than low density regions. The influence of human position on this data also makes hotspots closer to human activity (cities, major highways, roads) and thus more accessible for Devil capture.

Approximately 60 Devils will be captured and held in captivity, 15 Devils per test group. They will be properly housed in captivity for the duration of the study, following well known captivity guidelines practiced by Tasmanian Zoos and animal sanctuaries[43].

Imaging and Spectroscopy

In the first part of study 2, we will be using Magnetic Resonance Imaging (MRI) to compare the vasculature in Devil tissues over the four groups, as well as general tumour progression and size. Classical matter as we know it possesses several intrinsic properties; properties that are unique to the matter itself and not dependant on its relationship with any other matter or force[44]. Mass, for example, is an intrinsic property of matter, as is charge, since they are unique to matter that possesses them and will not change in response to any external force without the identity of the material changing. The lesser known, intrinsic property that MRI technology utilizes is *spin*.

Spin is perhaps a misnomer when describing the nature of particles since they do not actually 'spin' in the classical mechanical sense. We do not currently understand the mechanisms behind spin in a classical sense, however, we do know that particles behave as though they have an *intrinsic angular momentum* (spin), and so this property is immensely useful in our understanding of the world. As implied by the name, quantum physical systems are discrete, as is in the case of quantum spin. Any given particle may only possess either an up spin or a down spin, with a magnitude $\frac{\hbar}{2}$, where $\hbar$ is plank's constant h divided by 2π. Though only discretized states are allowed in quantum systems, transitional states are an allowed exception[45], as is in the case of quantum spin.

MRIs utilize quantum spin by leveraging its behaviour in a magnetic field. Specifically, hydrogen nuclei, or free protons, are used in MRI due it their abundance in the body. Since protons have intrinsic angular momentum and are charged particles, as stated by Lorenz's equation, they

exhibit a magnetic field. If this magnetic structure were to be placed in magnetic field, it would align with that field. In addition to the magnetic force, spin also gives the protons angular momentum, giving the particles a gyroscopic range of motion in a magnetic field. If the proton is tipped from its natural alignment with the magnetic field, it would precess in the direction of the magnetic field (Figure 9).

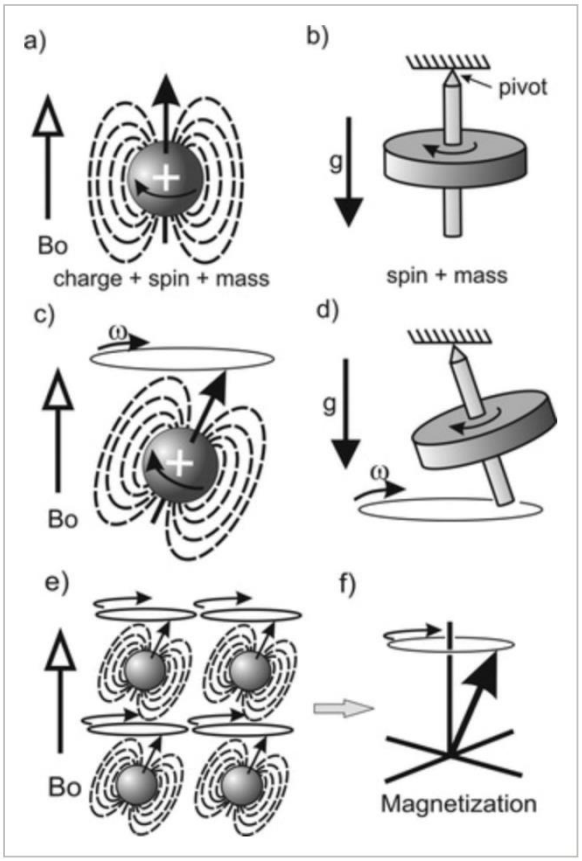

Figure 9. Schematic representing electron spin compared to a spinning top as an analog for the effective gyroscopic nature caused by intrinsic angular momentum in a magnetic field. When a top placed on a pivot is subjected to gravity as a downwards force and then given an angular velocity, it will precess around its pivot point, or 'wobble'. A similar phenomenon can be observed with particle spin. A magnetic field and the force it exerts on the charged particle can be analogous to gravity, and spin can be analogous to angular momentum. Image credit Plewes [46].

To detect the precessing magnetization, a pair of receiver coils are used in the MRI machine, which are connected to amplifiers tuned in to the Larmor frequency [45]. The magnetic field will oscillate over time due to the rotation, inducing a small signal in the coils. Only the time varying component, or the transverse component of the magnetization may induce a signal in the coil, and so only the rotation component, or the longitudinal component in the x-y plane is detected, which is parallel to the magnetic field. As such, to generate an NMR signal, the magnetization is tipped away from the equilibrium alignment so a component in the transverse plane precesses, which is achieved by exposing the protons to an alternating magnetic field that has a frequency equal to the Larmor frequency. Many protons' oscillations must be in phase for a signal to be measured, however, the interaction of the magnetic fields between protons leads to their dephasing. Differences in the spatial distribution of the magnetic field within different bodily tissues means that they will have unique Larmor frequencies and dephase at different rates. The time it takes for signal loss consequent to the dephasing is called T2. The time at which signal is measured, or echo time, is chosen carefully by an MRI technician is dictated by T2 and is maximized to yield the highest contrast in tissues of interest. The amount of time it takes the protons to recover from the dephasing is called T1, and it dictates the TR, or recovery time between proton excitations, which is also to be carefully chosen by the technician. Having a firm understanding of tissue properties as well as the physics concepts that inform MRI technology allows us to make measurements of specific tissues of interest.

In our study, a 3 tesla MRI will be used to assess facial vasculature in the four Devil demographics. A three tesla MRI was chosen due to the nature of the tissues being sampled. Since blood and muscle will be the primary tissues being compared, and there is such a high contrast in the tissue T2 (1932 ± 85 and 32 ± 2 respectively)[47,48], a stronger magnetic field is not necessary to provide adequate contrast. As such, a T2-weighted scan was chosen over a T1 weighted scan as the resulting tissue contrast is higher (T1 for blood is 275 ± 50[47], and T1 for muscle is 1295 ± 83[48]). The ideal echo time was then found by maximizing the difference between the free induction decay functions (*Appendix 4*). The resulting echo time was found to be 133.4 milliseconds (Figure 10).

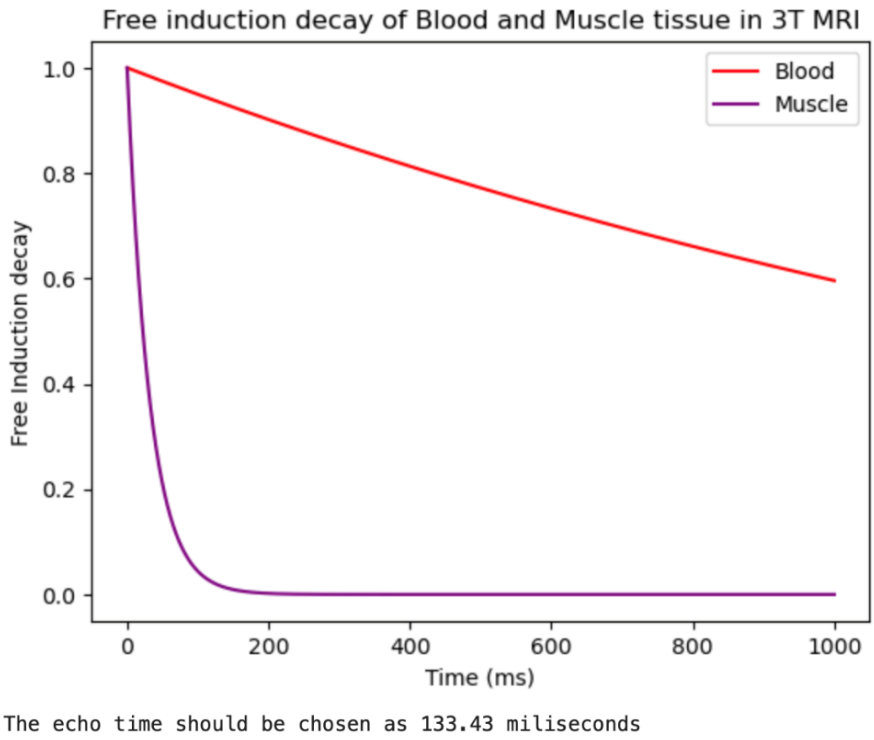

Figure 10. Plot of proton alignment decay functions (TR) for blood and muscle. The equation used was a version of decay as a function of time by transitioning to the rotating frame, which simplifies the expression, which becomes. The x-axis is the time in milliseconds since the start of the scan, the y-axis is the free induction decay. A is a constant representing the number of spins, sin of the flip angle, gyromagnetic ratio, and magnetic field. ω represents the angular velocity of the protons. Once the equation is simplified, T2 alone may be used to determine the echo time of the tissues. Figure created by Croft.

Once the Devil demographic groups have been examined using the above MRI technique, the vasculature density may be measured by rendering the 3D isosurfaces in the program Amira, as in Qi et al's study on vasculature in tumour growth. Amira is a medical software that takes imaging data, processes it and quantifies image characteristics like volumes, areas, perimeters[49]. Additionally, it may perform data registration, statistics, distribution graphs and 3D localization. The vasculature density of the infected / treated, uninfected / treated, infected / untreated and uninfected / untreated groups can then be compared using this software. From that, we may make a bar graph comparing the averages of each demographic's tumour density, as well as histograms

of each demographic's tumour density distributions. Finally, we may draw conclusions on the relationships that DFTD and the treatment have of tissue vasculature. MRI examination may also provide qualitative observations on tumour growth and progression between the infected / treated and infected / untreated groups to determine any visual effects of treatment.

Puncture Test

In the second part of study 2, we will examine the tissue strength of the four Devil groups and the relationship between vasculature from data previously collected using MRI and tissue puncture strength. This will be done by recreating the bites of Tasmanian Devils in the lab on epithelial tissue biopsies collected from each of the Devil groups. To recreate the maximum bite force of a Tasmanian Devil, we will be acquiring a mini hydraulic press capable of a maximum of 553N. That way, we can reliably repeat Devil bites in the laboratory[50]. A mini hydraulic press is not only inexpensive compared to a regular hydraulic press, but it is more capable of producing more sensitive force measurements to read the minimum force required to break the epithelial sample layers. To accommodate for the pressure differences, we will alter the surface area to replicate that of a Tasmanian Devil tooth. The simplest way to do this would be through the extraction of a tooth from a recently deceased Devil in the wild by utilizing the population data visualized by GIS. By attaching this to the hydraulic press, we can have an accurate recreation of a Devil's bite which is even further representative of the increased force per meter squared present in the skin. Our null hypothesis is if skin integrity remains the same in untreated vs treated Devils, then our model will remain unchanged and have the same projection. If the treated tumour samples demonstrate higher skin integrity than the untreated tumours, this would beneficially lower rates of transmission within Devil populations. The final case is if skin integrity is lower with the implementation of the drug. A recorded symptom of sunitinib is higher blood pressure[27]. Increased blood pressure typically results in decreased vasculature within the targeted tumour cells. This will ultimately create hypoxic tissue. Through further research, we will determine if the decreases in skin integrity are higher, equal to, or lower compared to pretreatment. The results of these samples will then influence our compartment-based model and treatment beyond the lab.

Conclusions and Perspectives

As scientists, it is our job not just to create knowledge but to apply it. Tasmanian Devils are a pillar of the local biodiversity and ecological integrity in Tasmania, and as such it is worthwhile allotting valuable time and resources to treating DFTD. Conservation efforts are necessary to ensure the long-term survival of Tasmanian Devils because a significant reduction in population could leave them susceptible to extinction by other means. Though species protection on its own is more than enough reason to save the Devils, our research also has implications in human health and cancer research.

In its existing state, we have found that DFTD does not pose the threat of extinction, however, DFTD will still massively diminish population size and genetic diversity, creating susceptibility to many other natural dangers, namely other pathogens, and cancers. The objective of study 1 was to thus find an effective strategy of DFDT eradication, which can be accomplished through proactive treatment of 67% of the current population.

Study 2 is then proposed to address sunitinib's unwanted, potential antagonistic effects on treatment. Sunitinib's effect on tumour vasculature and tissue integrity, and the potential alterations to transmissibility that arise from these must be understood if sunitinib is to stand as viable treatment to DFTD.

By understanding repeated forces dealt with by the body the concept of vasculature and tissue integrity can be applied for long-term vigorous exercise performed by cancer patients. Overall, regular exercise is seen as a good way of reducing stress and reducing many unwanted side effects in cancer patients[51] like chronic tiredness and high blood pressure[27]. There is limited information on the effects of long-term vigorous exercise for human patients under sunitinib. The trials of non-cancerous Devils under treatment will tell us the impact of our chemotherapeutic on tissue integrity. This will ultimately help regulate the capacity of long-term exercise performed by recovering cancer patients[52]. By understanding repeated forces dealt withstood by the body the concept of vasculature and skin integrity can be applied for long-term vigorous exercise performed by cancer patients.

If our results support sunitinib as a viable treatment for DFTD, it can be phased into larger scale distribution and use for the Devils. With updated information from our potentially altered model, the Tasmanian Devil population can be administered sunitinib using oral bait, distributed based on GIS observation and analysis. This can be done in accordance with the methods of the USDA oral rabies vaccination program, a large-scale raccoon vaccination project distributing 6.5 million oral rabies vaccinations yearly, spanning the entire U.S.A since 1995[53]. Oral baits can be engineered to the taste preferences of Tasmanian Devils to encourage consistent treatment.

By conducting a study on both the ecological effects of the disease and the treatment, as well as looking at the treatment's effects on vasculature and tissue strength, we can determine the best course of action going forward for the Devils- and protect the biodiversity of Tasmania.

References

1. Brüniche-Olsen A, Jones ME, Austin JJ, Burridge CP, Holland BR. Extensive population decline in the Tasmanian devil predates European settlement and devil facial tumour disease. *Biol Lett*. 2014;10(11):20140619. doi:10.1098/rsbl.2014.0619

2. Bender HS. Devil Facial Tumour Disease (DFTD): Using Genetics and Genomics to Investigate Infectious Disease in an Endangered Marsupial. *Marsupial Genetics and Genomics*. Published online February 20, 2010:499-515. doi:10.1007/978-90-481-9023-2_23

3. Hamede RK, McCallum H, Jones M. Biting injuries and transmission of Tasmanian devil facial tumour disease. *Journal of Animal Ecology*. 2013;82(1):182-190. doi:10.1111/j.1365-2656.2012.02025.x

4. Woods GM, Fox S, Flies AS, et al. Two Decades of the Impact of Tasmanian Devil Facial Tumor Disease. *Integrative and Comparative Biology*. 2018;58(6):1043-1054. doi:10.1093/icb/icy118

5. Pye R, Hamede R, Siddle HV, et al. Demonstration of immune responses against devil facial tumour disease in wild Tasmanian devils. *Biol Lett*. 2016;12(10):20160553. doi:10.1098/rsbl.2016.0553

6. Morris K, Austin JJ, Belov K. Low major histocompatibility complex diversity in the Tasmanian devil predates European settlement and may explain susceptibility to disease epidemics. *Biol Lett*. 2013;9(1):20120900. doi:10.1098/rsbl.2012.0900

7. Woods GM, Lyons AB, Bettiol SS. A Devil of a Transmissible Cancer. *TropicalMed*. 2020;5(2):50. doi:10.3390/tropicalmed5020050

8. Tissot S, Gérard AL, Boutry J, et al. Transmissible Cancer Evolution: The Under-Estimated Role of Environmental Factors in the “Perfect Storm” Theory. *Pathogens*. 2022;11(2):241. doi:10.3390/pathogens11020241

9. Taylor RL, Zhang Y, Schöning JP, Deakin JE. Identification of candidate genes for devil facial tumour disease tumourigenesis. *Sci Rep*. 2017;7(1):8761. doi:10.1038/s41598-017-08908-9

10. Charles A Janeway J, Travers P, Walport M, Shlomchik MJ. The major histocompatibility complex and its functions. In: *Immunobiology: The Immune System in Health and Disease. 5th Edition*. Garland Science; 2001. Accessed March 13, 2024. https://www.ncbi.nlm.nih.gov/books/NBK27156/

11. Taylor BC, Balko JM. Mechanisms of MHC-I Downregulation and Role in Immunotherapy Response. *Front Immunol*. 2022;13:844866. doi:10.3389/fimmu.2022.844866

12. Pfizer Labs. *SUTENT® (SUNITINIB MALATE) CAPSULES*.; 2006:20. https://www.accessdata.fda.gov/drugsatfda_docs/label/2006/021968lbl.pdf

13. Abreu E, Amir A, Chibba A, et al. 4.3 – Aromaticity. Published online July 13, 2023. Accessed April 3, 2024. https://ecampusontario.pressbooks.pub/mcmasterchem1aa3/chapter/4-3-aromaticity/2/

14. PubChem. Sunitinib. Accessed March 25, 2024. https://pubchem.ncbi.nlm.nih.gov/compound/5329102

15. Vallejo Narváez WE, Jiménez EI, Romero-Montalvo E, et al. Acidity and basicity interplay in amide and imide self-association †Electronic supplementary information (ESI) available: Experimental and computational details. Protocol for the recording of 1H-DOSY and 1H-NMR titrations (A1, A2, A4–A7, I1–I5 and I8). Correlations of the computed acidity and basicity with experimental data. Molecular graphs of the monomers and dimers of amides and imides computed with SMD-M06-2x/6-311++G(2d,2p) electron densities. Characterisation of selected HBs in terms of the topological properties of ρ(r) such as delocalisation index and the Interacting Quantum Atoms energy partition. XYZ coordinates and electronic energies of all species addressed in the paper. See DOI: 10.1039/c8sc01020j. *Chem Sci*. 2018;9(19):4402-4413. doi:10.1039/c8sc01020j

16. Wang E, DuBois SG, Wetmore C, Verschuur AC, Khosravan R. Population Pharmacokinetics of Sunitinib and its Active Metabolite SU012662 in Pediatric Patients with Gastrointestinal Stromal Tumors or Other Solid Tumors. *Eur J Drug Metab Pharmacokinet*. 2021;46(3):343-352. doi:10.1007/s13318-021-00671-7

17. Chapter 1 Pharmacokinetics & Pharmacodynamics - Nursing Pharmacology - NCBI Bookshelf. Accessed April 4, 2024. https://www.ncbi.nlm.nih.gov/books/NBK595006/

18. Deeks ED, Keating GM. Sunitinib. *Drugs*. 2006;66(17):2255-2266. doi:10.2165/00003495-200666170-00007

19. Optimizing the dose in cancer patients treated with imatinib, sunitinib and pazopanib - Lankheet - 2017 - British Journal of Clinical Pharmacology - Wiley Online Library. Accessed April 3, 2024. https://bpspubs.onlinelibrary.wiley.com/doi/full/10.1111/bcp.13327

20. Li X, Jiang W, Dong S, Li W, Zhu W, Zhou W. STAT3 Inhibitors: A Novel Insight for Anticancer Therapy of Pancreatic Cancer. *Biomolecules*. 2022;12(10):1450. doi:10.3390/biom12101450

21. Roskoski R. Sunitinib: A VEGF and PDGF receptor protein kinase and angiogenesis inhibitor. *Biochemical and Biophysical Research Communications*. 2007;356(2):323-328. doi:10.1016/j.bbrc.2007.02.156

22. Chen SH, Murphy D, Lassoued W, Thurston G, Feldman MD, Lee WMF. Activated STAT3 is a mediator and biomarker of VEGF endothelial activation. *Cancer Biology & Therapy*. 2008;7(12):1994-2003. doi:10.4161/cbt.7.12.6967

23. Yan JF, Huang WJ, Zhao JF, et al. The platelet-derived growth factor receptor/STAT3 signaling pathway regulates the phenotypic transition of corpus cavernosum smooth muscle in rats. Pintus G, ed. *PLoS ONE*. 2017;12(2):e0172191. doi:10.1371/journal.pone.0172191

24. Wang J, Guo XJ, Ding YM, Jiang JX. miR-1181 inhibits invasion and proliferation *via* STAT3 in pancreatic cancer. *WJG*. 2017;23(9):1594. doi:10.3748/wjg.v23.i9.1594

25. Li Y, Sarkar FH. MicroRNA Targeted Therapeutic Approach for Pancreatic Cancer. *Int J Biol Sci*. 2016;12(3):326-337. doi:10.7150/ijbs.15017

26. Cui Y, Huang L, Elefteriou F, et al. Essential Role of STAT3 in Body Weight and Glucose Homeostasis. *Molecular and Cellular Biology*. 2004;24(1):258-269. doi:10.1128/MCB.24.1.258-269.2004

27. Dreicer R. Management of side effects associated with sunitinib therapy for patients with renal cell carcinoma. *OTT*. Published online March 2009:51. doi:10.2147/OTT.S4052

28. Jones ME, Paetkau D, Geffen E, Moritz C. Genetic diversity and population structure of Tasmanian devils, the largest marsupial carnivore. *Mol Ecol*. 2004;13(8):2197-2209. doi:10.1111/j.1365-294X.2004.02239.x

29. Gallagher S, Eddy WF. Comparing compartment and agent-based models. Published online October 25, 2017.

30. Keeley T, O'Brien JK, Fanson BG, Masters K, McGreevy PD. The reproductive cycle of the Tasmanian devil (*Sarcophilus harrisii*) and factors associated with reproductive success in captivity. *General and Comparative Endocrinology*. 2012;176(2):182-191. doi:10.1016/j.ygcen.2012.01.011

31. Keeley T, Russell T, Carmody K, et al. Seasonality and breeding success of captive and wild Tasmanian devils (*Sarcophilus harrisii*). *Theriogenology*. 2017;95:33-41. doi:10.1016/j.theriogenology.2017.02.013

32. Quantifying 25 years of disease-caused declines in Tasmanian devil populations: host density drives spatial pathogen spread - PMC. Accessed April 3, 2024. https://www.ncbi.nlm.nih.gov/pmc/articles/PMC9844790/

33. Hendricks S, Epstein B, Schönfeld B, et al. Conservation implications of limited genetic diversity and population structure in Tasmanian devils (Sarcophilus harrisii). *Conserv Genet*. 2017;18(4):977-982. doi:10.1007/s10592-017-0939-5

34. McLennan EA, Gooley RM, Wise P, Belov K, Hogg CJ, Grueber CE. Pedigree reconstruction using molecular data reveals an early warning sign of gene diversity loss in an island population of Tasmanian devils (Sarcophilus harrisii). *Conserv Genet*. 2018;19(2):439-450. doi:10.1007/s10592-017-1017-8

35. van den Driessche P. Reproduction numbers of infectious disease models. *Infect Dis Model*. 2017;2(3):288-303. doi:10.1016/j.idm.2017.06.002

36. Gregory Cousins. GitHub - gregcousins/Economic-Modeling-of-STD-Transmission: We propose some simple compartmental models to estimal the savings possible by investing in tests with faster result time. GitHub. Accessed March 23, 2024. https://github.com/gregcousins/Economic-Modeling-of-STD-Transmission

37. Shahin H, Elmasry M, Steinvall I, Söberg F, El-Serafi A. Vascularization is the next challenge for skin tissue engineering as a solution for burn management. *Burns Trauma*. 2020;8:tkaa022. doi:10.1093/burnst/tkaa022

38. Tumor-Specific Diagnostic Marker for Transmissible Facial Tumors of Tasmanian Devils: Immunohistochemistry Studies - C. Tovar, D. Obendorf, E. P. Murchison, A. T. Papenfuss, A. Kreiss, G. M. Woods, 2011. Accessed April 3, 2024. https://journals.sagepub.com/doi/10.1177/0300985811400447

39. Rodríguez J, Castañeda G, Muñoz L, Villa JC. Quantitation of sunitinib, an oral multitarget tyrosine kinase inhibitor, and its metabolite in urine samples by nonaqueous capillary electrophoresis time of flight mass spectrometry. *ELECTROPHORESIS*. 2015;36(14):1580-1587. doi:10.1002/elps.201400588

40. Qin Z, Liu HM, Ma YX, Wang XD. Chapter 9 - Developments in extraction, purification, and structural elucidation of proanthocyanidins (2000–2019). In: Atta-ur-Rahman, ed. *Studies in Natural Products Chemistry*. Vol 68. Bioactive Natural Products. Elsevier; 2021:347-391. doi:10.1016/B978-0-12-819485-0.00008-6

41. Space use and temporal partitioning of sympatric Tasmanian devils and spotted-tailed quolls - Andersen - 2020 - Austral Ecology - Wiley Online Library. Accessed April 3, 2024. https://onlinelibrary.wiley.com/doi/full/10.1111/aec.12865

42. NVA. Natural Values Atlas. Accessed March 27, 2024. https://www.naturalvaluesatlas.tas.gov.au/#SpeciesObservationSearchPage

43. Yumpu.com. Tasmanian devil - mammalia - Nswfmpa.org. yumpu.com. Accessed April 3, 2024. https://www.yumpu.com/en/document/read/43848509/tasmanian-devil-mammalia-nswfmpaorg

44. Sider T. Intrinsic Properties. *Philosophical Studies: An International Journal for Philosophy in the Analytic Tradition*. 1996;83(1):1-27.

45. Plewes DB, Kucharczyk W. Physics of MRI: A primer. *Journal of Magnetic Resonance Imaging*. 2012;35(5):1038-1054. doi:10.1002/jmri.23642

46. Physics of MRI: A primer - Plewes - 2012 - Journal of Magnetic Resonance Imaging - Wiley Online Library. Accessed April 2, 2024. https://onlinelibrary.wiley.com/doi/10.1002/jmri.23642

47. Stanisz GJ, Odrobina EE, Pun J, et al. T1, T2 relaxation and magnetization transfer in tissue at 3T. *Magnetic Resonance in Medicine*. 2005;54(3):507-512. doi:10.1002/mrm.20605

48. Gold GE, Han E, Stainsby J, Wright G, Brittain J, Beaulieu C. Musculoskeletal MRI at 3.0 T: Relaxation Times and Image Contrast. *American Journal of Roentgenology*. 2004;183(2):343-351. doi:10.2214/ajr.183.2.1830343

49. Amira Software for cell biology - CA. Accessed April 3, 2024. https://www.thermofisher.com/ca/en/home/electron-microscopy/products/software-em-3d-vis/amira-software/cell-biology.html

50. Tasmanian devil (Sarcophilus harrisii) - JungleDragon. Accessed March 29, 2024. https://www.jungledragon.com/specie/2656/tasmanian_devil.html

51. De Lazzari N, Niels T, Tewes M, Götte M. A Systematic Review of the Safety, Feasibility and Benefits of Exercise for Patients with Advanced Cancer. *Cancers (Basel)*. 2021;13(17):4478. doi:10.3390/cancers13174478

52. Deptuła M, Zieliński J, Wardowska A, Pikuła M. Wound healing complications in oncological patients: perspectives for cellular therapy. *Postepy Dermatol Alergol*. 2019;36(2):139-146. doi:10.5114/ada.2018.72585

53. Oral Rabies Vaccination | Animal and Plant Health Inspection Service. Accessed April 3, 2024. https://www.aphis.usda.gov/national-wildlife-programs/rabies/vaccine

Appendices

Appendix A

$$L_D = V_d * C_s / F$$

$$L_D = 2230{,}000 \text{ ml} * 101\text{x}10^{-9}\text{g*ml}^{-1} / 0.95$$

$$L_D = 237 \text{ mg}$$

Loading dose is equal to the volume of distribution (which is the volume as to which the drug is dispersing into) multiplied by the plasma drug concentration which is the concentration of the drug at steady state by the maximum concentration. Then divided by the bioavailability which is 0.95 for an oral drug.

Appendix B

$$L_D = V_d * C_s / F$$

$$L_D = 2230{,}000 \text{ ml} * 62.9\text{x}10^{-9}\text{g*ml}^{-1} / 0.95$$

$$L_D = 147 \text{ mg}$$

Loading dose is equal to the volume of distribution (which is the volume as to which the drug is dispersing into) multiplied by the plasma drug concentration which is the concentration of the drug at steady state at the lower range. Then divided by the bioavailability which is 0.95 for an oral drug.

Appendix C

$$M_D = Cl_R * C_s / F$$

$$M_D = 62000 \text{ ml/h} * 101x10^{-9}\text{g/ml} / 1$$

$$= 6.26 \text{ mg/h}$$

Maintenance dose which is represented by M_D is equal to Cl_R which is clearance rate of the drug exiting the body, C_s is the target concentration that would achieve steady state and F is bioavailability of the drug[16].

Appendix D

```
import numpy as np
import matplotlib.pyplot as plt
from scipy.integrate import odeint
a = 0
b = 400
n = 400
t = np.linspace(a, b, n)
def compartment(y, t, hourly_dose, clearance_s, clearace_m, absorption, metabolism, distribution_s, distribution_m):
    GI, S, M = y

    dGIdt = hourly_dose - absorption * GI

    dSdt = absorption * GI - clearance_s * S / distribution_s

    dMdt = metabolism * S - clearance_m * M / distribution_m
    return [dGIdt, dSdt, dMdt]
clearance_s = 48  #L/hr

clearance_m =  29.6 #L/hr

hourly_dose = 2.083 #mg/hour

metabolism = 0.01

absorption = 0.95

distribution_s = 2230

distribution_m = 3080

y0 = [237, 0, 0]

#fix graph for report

protosolution = odeint(compartment, y0, t, args=(hourly_dose, clearance_s, clearance_m, absorption, metabolism, distribution_s, distribution_m))

GI, S, M = protosolution.T  # Extracting the first column from the solution array
plt.figure(figsize=(10, 6))
plt.plot(t, S, 'skyblue', label='Sunitinib', linewidth=2.5)
plt.plot(t, M, 'orange', label = 'Primary metabolite',linewidth=2.5)
plt.plot(t, S+M, 'green', label = 'Sum of sunitinib and its primary active metabolite',linewidth=2.5)
#plt.plot(t, GI, 'g', label = 'GI tract')
plt.title('Loading dose')
plt.axhline(y = 237, color = 'purple', linestyle = '-')
plt.axhline(y = 140, color = 'purple', linestyle = '-')
plt.xlabel('Time (hours)')
ax = plt.gca()
ax.set_xlim([0,400])
ax.set_ylim([0, 250])

plt.fill_between(t, 140,237, color = 'orchid', alpha = 0.25)
plt.ylabel('Amount of compound in the body (mg)')
plt.legend()
plt.legend
plt.grid(True)
plt.show()
```

```
t = np.linspace(a, b, n)


def compartment(y, t, hourly_dose, clearance_s, clearace_m, absorption, metabolism, distribution_s, distribution_m):
    GI, S, M = y
    dGIdt = hourly_dose - absorption * GI
    dSdt = absorption * GI - clearance_s * S / distribution_s
    dMdt = metabolism * S - clearance_m * M / distribution_m

    return [dGIdt, dSdt, dMdt]


clearance_s = 48  #L/hr
clearance_m =  29.6 #L/hr
hourly_dose = 2.083 #mg/hour
metabolism = 0.01
absorption = 0.95
distribution_s = 2230
distribution_m = 3080
y0 = [50, 0, 0]
#fix graph for report
protosolution = odeint(compartment, y0, t, args=(hourly_dose, clearance_s, clearance_m, absorption, metabolism, distribution_s, distribution_m))
GI, S, M = protosolution.T  # Extracting the first column from the solution array


plt.figure(figsize=(10, 6))
plt.plot(t, S, 'skyblue', label='Sunitinib',linewidth=2.5)
plt.plot(t, M, 'orange', label = 'Primary metabolite',linewidth=2.5)
plt.plot(t, S+M, 'g', label = 'Sum of sunitinib and its primary active metabolite',linewidth=2.5)
#plt.plot(t, GI, 'g', label = 'GI tract')
plt.title('No Loading Dose')
plt.axhline(y = 237, color = 'purple', linestyle = '-')
plt.axhline(y = 140, color = 'purple', linestyle = '-')
plt.xlabel('Time (hours)')
ax = plt.gca()
ax.set_xlim([0,400])
ax.set_ylim([0, 250])
plt.fill_between(t, 140,237, color = 'orchid', alpha = 0.25)
plt.ylabel('Amount of compound in the body (mg)')
plt.legend()
plt.grid(True)
plt.show()
```

Code to create and display the compartment based pharmacokinetic model

Appendix E

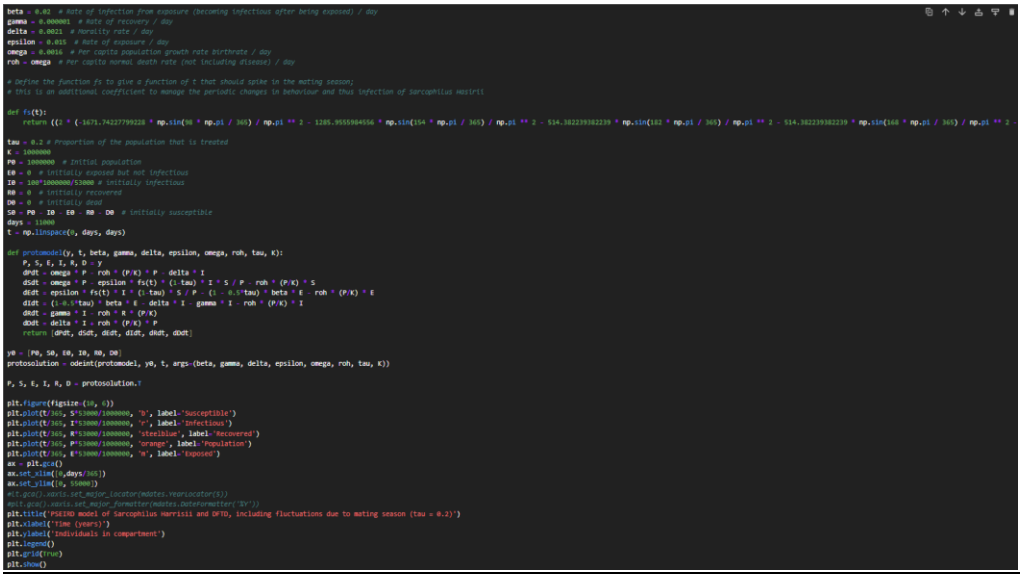

```
beta = 0.02  # Rate of infection from exposure (becoming infectious after being exposed) / day
gamma = 0.000001  # Rate of recovery / day
delta = 0.0021  # Mortality rate / day
epsilon = 0.01  # Rate of exposure / day
omega = 0.0016  # Per capita population growth rate birthrate / day
roh = omega  # Per capita normal death rate (not including disease) / day

# Define the function fs to give a function of t that should spike in the mating season;
# this is an additional coefficient to manage the periodic changes in behaviour and thus infection of Sarcophilus Harrisii

def fs(t):
    return ((3 * (-1671.742277992228 * np.sin(30 * np.pi / 365) / np.pi ** 2 - 1285.9555984556 * np.sin(154 * np.pi / 365) / np.pi ** 2 - 514.3822393982239 * np.sin(182 * np.pi / 365) / np.pi ** 2 - 514.3822393982239 * np.sin(168 * np.pi / 365) / np.pi ** 2 -

tau = 0.2 # Proportion of the population that is treated
K = 1000000
P0 = 1000000  # Initial population
E0 = 0  # Initially exposed but not infectious
I0 = 100*1000000/53000 # Initially infectious
R0 = 0  # Initially recovered
D0 = 0  # Initially dead
S0 = P0 - I0 - E0 - R0 - D0  # Initially susceptible
days = 11000
t = np.linspace(0, days, days)

def protomodel(y, t, beta, gamma, delta, epsilon, omega, roh, tau, K):
    P, S, E, I, R, D = y
    dPdt = omega * P - roh * (P/K) * P - delta * I
    dSdt = omega * P - epsilon * fs(t) * (1-tau) * I * S / P - roh * (P/K) * S
    dEdt = epsilon * fs(t) * I * (1-tau) * S / P - (1 - 0.5*tau) * beta * E - roh * (P/K) * E
    dIdt = (1-0.5*tau) * beta * E - delta * I - gamma * I - roh * (P/K) * I
    dRdt = gamma * I - roh * R * (P/K)
    dDdt = delta * I - roh * (P/K) * P
    return [dPdt, dSdt, dEdt, dIdt, dRdt, dDdt]

y0 = [P0, S0, E0, I0, R0, D0]
protosolution = odeint(protomodel, y0, t, args=(beta, gamma, delta, epsilon, omega, roh, tau, K))

P, S, E, I, R, D = protosolution.T

plt.figure(figsize=(10, 6))
plt.plot(t/365, S*53000/1000000, 'b', label='Susceptible')
plt.plot(t/365, I*53000/1000000, 'r', label='Infectious')
plt.plot(t/365, R*53000/1000000, 'steelblue', label='Recovered')
plt.plot(t/365, P*53000/1000000, 'orange', label='Population')
plt.plot(t/365, E*53000/1000000, 'm', label='Exposed')
ax = plt.gca()
ax.set_xlim([0,days/365])
ax.set_ylim([0, 65000])
#ax.xaxis.set_major_locator(mdates.YearLocator(1))
#ax.xaxis.set_major_formatter(mdates.DateFormatter('%Y'))
plt.title('PSEIRD model of Sarcophilus Harrisii and DFTD, including fluctuations due to mating season (tau = 0.2)')
plt.xlabel('Time (years)')
plt.ylabel('Individuals in compartment')
plt.legend()
plt.grid(True)
plt.show()
```

Code to create and display the compartment-based model.

```
from sympy import Piecewise, symbols

def piecewisee(t):
    nr = 0.1  # Assuming nr is defined somewhere

    return Piecewise(
        (nr, t_symbol < 35),
        ((t_symbol/7 - 5)/37 + nr, (35 <= t_symbol) & (t_symbol < 42)),
        ((3*t_symbol/7 - 17)/37 + nr, (42 <= t_symbol) & (t_symbol < 49)),
        ((16*t_symbol/7 - 108)/37 + nr, (49 <= t_symbol) & (t_symbol < 56)),
        ((12*t_symbol/7 - 76)/37 + nr, (56 <= t_symbol) & (t_symbol < 63)),
        ((5*t_symbol/7 - 13)/37 + nr, (63 <= t_symbol) & (t_symbol < 70)),
        ((-19*t_symbol/7 + 227)/37 + nr, (70 <= t_symbol) & (t_symbol < 77)),
        ((-9*t_symbol/7 + 117)/37 + nr, (77 <= t_symbol) & (t_symbol < 84)),
        ((-5*t_symbol/7 + 69)/37 + nr, (84 <= t_symbol) & (t_symbol < 91)),
        ((-t_symbol/7 + 17)/37 + nr, (91 <= t_symbol) & (t_symbol < 98)),
        ((-t_symbol/7 + 17)/37 + nr, (98 <= t_symbol) & (t_symbol < 105)),
        ((-2*t_symbol/7 + 32)/37 + nr, (105 <= t_symbol) & (t_symbol < 112)),
        (nr, True)
    )
nr = 0.1
t_symbol = symbols('t_symbol')
p =smp.Piecewise((nr, t_symbol < 35),
        ((t_symbol/7 - 5)/37 + nr, (35 <= t_symbol) & (t_symbol < 42)),
        ((3*t_symbol/7 - 17)/37 + nr, (42 <= t_symbol) & (t_symbol < 49)),
        ((16*t_symbol/7 - 108)/37 + nr, (49 <= t_symbol) & (t_symbol < 56)),
        ((12*t_symbol/7 - 76)/37 + nr, (56 <= t_symbol) & (t_symbol < 63)),
        ((5*t_symbol/7 - 13)/37 + nr, (63 <= t_symbol) & (t_symbol < 70)),
        ((-19*t_symbol/7 + 227)/37 + nr, (70 <= t_symbol) & (t_symbol < 77)),
        ((-9*t_symbol/7 + 117)/37 + nr, (77 <= t_symbol) & (t_symbol < 84)),
        ((-5*t_symbol/7 + 69)/37 + nr, (84 <= t_symbol) & (t_symbol < 91)),
        ((-t_symbol/7 + 17)/37 + nr, (91 <= t_symbol) & (t_symbol < 98)),
        ((-t_symbol/7 + 17)/37 + nr, (98 <= t_symbol) & (t_symbol < 105)),
        ((-2*t_symbol/7 + 32)/37 + nr, (105 <= t_symbol) & (t_symbol < 112)),
        (nr, t_symbol>=112))
# Example usage
fs = smp.fourier_series(p, (t_symbol,0,365))
fs.truncate(4).simplify
```

Code to create the Fourier series to approximate the mating season behaviours of the Tasmanian Devils

Appendix F

To begin calculating $\mathcal{R}0$, we will review the model as described earlier in the proposal.

$$\frac{dS}{dt} = \omega N - \frac{\epsilon f_s (1-\tau) IS}{N} - \frac{\rho SN}{K}$$

$$\frac{dE}{dt} = \frac{\epsilon f_s I(1-\tau)S}{N} - (1-0.5\tau)\beta E - \frac{\rho EN}{K}$$

$$\frac{dI}{dt} = (1-0.5\tau)\beta E - \delta I - \frac{\gamma I - \rho IN}{K}$$

$$\frac{dR}{dt} = \gamma I - \frac{\rho RN}{K}$$

Each of these rates of change is written in the standard form Fc-Vc, where Fc is the rate of new infections into the compartment and Vc is the rate into compartment by means other than infection, where C is the individual compartment and exists for all compartments. Let Fi and Vi be as follows:

Fi : $\begin{bmatrix} \frac{IS\epsilon f_s(1-\tau)}{N} \\ 0 \\ 0 \end{bmatrix}$ Vi : $\begin{bmatrix} \frac{EN\rho}{k} + E\beta(1-0.5\tau) \\ -E\beta(1-0.5\tau) + \frac{IN\rho}{k} + I\delta + I\gamma \\ -I\gamma + \frac{NR\rho}{k} \end{bmatrix}$

To continue computing $\mathcal{R}0$, the disease free equilibrium will be substituted into the vectors Fc and Vc. The disease free equilibrium is the population equilibrium where no individuals have been infected. The disease free equilibrium for our model exists such that all of the population is

$\begin{bmatrix} 0 & \epsilon f_s(1-\tau) & 0 \\ 0 & 0 & 0 \\ 0 & 0 & 0 \end{bmatrix}$ $\begin{bmatrix} \frac{N\rho}{k} + \beta(1-0.5\tau) & 0 & 0 \\ -\beta(1-0.5\tau) & \frac{N\rho}{k} + \delta + \gamma & 0 \\ 0 & -\gamma & \frac{N\rho}{k} \end{bmatrix}$

susceptible, none is exposed, none is infectious and none is recovered. Now, the Jacobians of Fi and Vi are F and V respectively, as follows :

The next step in the next generation matrix method is to multiply the matrices F and V^{-1} to create a new matrix K. K is as follows :

$$\begin{bmatrix} \frac{\epsilon f_s(1-\tau)(0.5\beta k^2\tau-1.0\beta k^2)}{-1.0N^2\rho^2+0.5N\beta k\rho\tau-1.0N\beta k\rho-1.0N\delta k\rho-1.0N\gamma k\rho+0.5\beta\delta k^2\tau-1.0\beta\delta k^2+0.5\beta\gamma k^2\tau-1.0\beta\gamma k^2} & \frac{0.5\epsilon f_s k(1-\tau)}{0.5N\rho+0.5\delta k+0.5\gamma k} & 0 \\ 0 & 0 & 0 \\ 0 & 0 & 0 \end{bmatrix}$$

The last step is to determine the greatest eigenvalue of this matrix, which is the first entry. Therefore we can come to the conclusion that $\mathcal{R}0$ when simplified is as follows:

$$\mathcal{R}_0 = \frac{\beta\epsilon f_s k^2(1-0.5\tau)(1-\tau)}{(N\rho+k\delta+k\gamma)(N\rho-0.5k\beta\tau+k\beta)}$$

Each of these individual parameters can be substituted for using the determined parameters in the model, yielding a time dependent $\mathcal{R}0$ that is discussed in text. Thank you to Dr. Gregory Cousins for the GitHub repository, that made these calculations much easier.

Appendix G

```
[30]: import numpy as np
      import matplotlib.pyplot as plt
      import sympy as sp

      def st_blood(t):
          stb = np.exp(-t/1932)
          return stb

      def st_muscle(t):
          stm = np.exp(-t/32)
          return stm

      def comp_blood_and_msucle(t):
          stc = np.exp(-t/1932) - np.exp(-t/32)
          return stc

      t = np.linspace(0, 1000, 100000)
      deriv = (-t/1932)*np.exp(-t/1932)+(t/32)*np.exp(-t/32)

      plt.plot(t, st_blood(t), label='Blood', color ='red')
      plt.plot(t, st_muscle(t), label='Muscle', color = 'purple')
      #plt.plot(t, deriv, label='slope')
      #plt.plot(t,comp_blood_and_msucle(t), label='composite' )
      plt.xlabel("Time (ms)")
      plt.ylabel("Free Induction decay")
      plt.title("Free induction decay of Blood and Muscle tissue in 3T MRI")
      plt.legend()
      plt.show()

      print('The echo time should be chosen as', np.argmax((np.exp(-t/1932) - np.exp(-t/32)))/100,'miliseconds')
```

Python code for echo time calculations and decay graphs